

Fusion at near-barrier energies within quantum diffusion approach

V.V.Sargsyan¹, G.G.Adamian¹, N.V.Antonenko¹, W. Scheid², and H.Q.Zhang³

¹*Joint Institute for Nuclear Research, 141980 Dubna, Russia*

²*Institut für Theoretische Physik der Justus-Liebig-Universität, D-35392 Giessen, Germany*

³*China Institute of Atomic Energy, Post Office Box 275, Beijing 102413, China*

(Dated: July 11, 2018)

Within the quantum diffusion approach the role of neutron transfer in the fusion (capture) reactions with toughly and weakly bound nuclei is discussed. The breakup process is analyzed. New methods for the study of the breakup probability are suggested.

I. INTRODUCTION

The nuclear deformation and neutron-transfer process have been identified as playing a major role in the magnitude of the sub-barrier fusion (capture) cross sections [1]. There are a several experimental evidences which confirm the importance of nuclear deformation on the fusion. The influence of nuclear deformation is straightforward. If the target nucleus is prolate in the ground state, the Coulomb field on its tips is lower than on its sides, that then increases the capture or fusion probability at energies below the barrier corresponding to the spherical nuclei. The role of neutron transfer reactions is less clear. The importance of neutron transfer with positive Q -values on nuclear fusion (capture) originates from the fact that neutrons are insensitive to the Coulomb barrier and therefore they can start being transferred at larger separations before the projectile is captured by target-nucleus. Therefore, it is generally thought that the sub-barrier fusion cross section will increase because of the neutron transfer.

The fusion (capture) dynamics induced by loosely bound radioactive ion beams is currently being extensively studied. However, the long-standing question whether fusion (capture) is enhanced or suppressed with these beams has not yet been answered unambiguously. The study of the fusion reactions involving nuclei at the drip-lines has led to contradictory results.

II. QUANTUM DIFFUSION APPROACH FOR CAPTURE

In the quantum diffusion approach [2–6] the capture of the projectile by the target-nucleus is described with a single relevant collective variable: the relative distance between the colliding nuclei. This approach takes into consideration the fluctuation and dissipation effects in collisions of heavy ions which model the coupling of the relative motion with various channels (for example, the non-collective single-particle excitations, low-lying collective dynamical modes of the target and projectile). The nuclear static deformation effects are taken into account through the dependence of the nucleus-nucleus potential on the deformations and mutual orientations of the colliding nuclei. We have to mention that many quantum-mechanical and non-Markovian effects accompanying the passage through the potential barrier are taken into consideration in our formalism [2, 4].

The capture cross section is a sum of partial capture cross sections [2, 4]

$$\begin{aligned}\sigma_{cap}(E_{c.m.}) &= \sum_J \sigma_{cap}(E_{c.m.}, J) = \\ &= \pi \lambda^2 \sum_J (2J+1) \int_0^{\pi/2} d\theta_1 \sin(\theta_1) \int_0^{\pi/2} d\theta_2 \sin(\theta_2) P_{cap}(E_{c.m.}, J, \theta_1, \theta_2),\end{aligned}\quad (1)$$

where $\lambda^2 = \hbar^2/(2\mu E_{c.m.})$ is the reduced de Broglie wavelength, $\mu = m_0 A_1 A_2 / (A_1 + A_2)$ is the reduced mass (m_0 is the nucleon mass), and the summation is over the possible values of angular momentum J at a given bombarding energy $E_{c.m.}$. Knowing the potential of the interacting nuclei for each orientation with the angles θ_i ($i = 1, 2$), one can obtain the partial capture probability P_{cap} which is defined by the passing probability of the potential barrier in the relative distance R coordinate at a given J . The value of P_{cap} is obtained by integrating the propagator G from the initial state (R_0, P_0) at time $t = 0$ to the final state (R, P) at time t (P is a momentum):

$$P_{cap} = \lim_{t \rightarrow \infty} \int_{-\infty}^{r_{in}} dR \int_{-\infty}^{\infty} dP G(R, P, t | R_0, P_0, 0) = \lim_{t \rightarrow \infty} \frac{1}{2} \operatorname{erfc} \left[\frac{-r_{in} + \overline{R(t)}}{\sqrt{\Sigma_{RR}(t)}} \right].\quad (2)$$

The second line in (2) is obtained by using the propagator $G = \pi^{-1} |\det \Sigma^{-1}|^{1/2} \exp(-\mathbf{q}^T \Sigma^{-1} \mathbf{q})$ ($\mathbf{q}^T = [q_R, q_P]$, $q_R(t) = R - \overline{R(t)}$, $q_P(t) = P - \overline{P(t)}$, $\overline{R(t=0)} = R_0$, $\overline{P(t=0)} = P_0$, $\Sigma_{kk'}(t) = 2q_k(t)q_{k'}(t)$, $\Sigma_{kk'}(t=0) = 0$),

$k, k' = R, P$) calculated for an inverted oscillator which approximates the nucleus-nucleus potential V in the variable R . The frequency ω of this oscillator with an internal turning point r_{in} is defined from the condition of equality of the classical actions of approximated and realistic potential barriers of the same height at given J . This approximation is well justified for the reactions and energy range, which are here considered.

We assume that the sub-barrier capture mainly depends on the optimal one-neutron ($Q_{1n} > Q_{2n}$) or two-neutron ($Q_{2n} > Q_{1n}$) transfer with the positive Q -value. Our assumption is that, just before the projectile is captured by the target-nucleus (just before the crossing of the Coulomb barrier) which is a slow process, the transfer occurs and can lead to the population of the first excited collective state in the recipient nucleus [7] (the donor nucleus remains in the ground state). So, the motion to the N/Z equilibrium starts in the system before the capture because it is energetically favorable in the dinuclear system in the vicinity of the Coulomb barrier. For the reactions under consideration, the average change of mass asymmetry is connected to the one- or two-neutron transfer ($1n$ - or $2n$ -transfer). Since after the transfer the mass numbers, the isotopic composition and the deformation parameters of the interacting nuclei, and, correspondingly, the height $V_b = V(R_b)$ and shape of the Coulomb barrier are changed, one can expect an enhancement or suppression of the capture. If after the neutron transfer the deformations of interacting nuclei increase (decrease), the capture probability increases (decreases). When the isotopic dependence of the nucleus-nucleus potential is weak and after the transfer the deformations of interacting nuclei do not change, there is no effect of the neutron transfer on the capture. In comparison with Ref. [8], we assume that the negative transfer Q -values do not play visible role in the capture process. Our scenario was verified in the description of many reactions [4–6].

III. RESULTS OF CALCULATIONS

Because the capture cross section is equal to the complete fusion cross section for the reactions treated, the quantum diffusion approach for the capture is applied to study the complete fusion. All calculated results are obtained with the same set of parameters as in Ref. [2]. Realistic friction coefficient in the relative distance coordinate $\hbar\lambda=2$ MeV is used. Its value is close to that calculated within the mean-field approaches [9]. For the nuclear part of the nucleus-nucleus potential, the double-folding formalism with the Skyrme-type density-dependent effective nucleon-nucleon interaction is used [2, 4]. The parameters of the nucleus-nucleus interaction potential $V(R)$ are adjusted to describe the experimental data at energies above the Coulomb barrier corresponding to spherical nuclei. The absolute values of the experimental quadrupole deformation parameters β_2 of even-even deformed nuclei in the ground state and of the first excited collective states of nuclei are taken from Ref. [10]. For the nuclei deformed in the ground state, the β_2 in the first excited collective state is similar to the β_2 in the ground state. For the quadrupole deformation parameter of an odd nucleus, we choose the maximal value from the deformation parameters of neighboring even-even nuclei (for example, $\beta_2(^{231}\text{Th})=\beta_2(^{233}\text{Th})=\beta_2(^{232}\text{Th})=0.261$). For the double magic and neighboring nuclei, we take $\beta_2 = 0$ in the ground state. Since there are uncertainties in the definition of the values of β_2 in light-mass nuclei, one can extract the ground-state quadrupole deformation parameters of these nuclei from a comparison of the calculated capture cross sections with the existing experimental data. By describing the reactions $^{12}\text{C}+^{208}\text{Pb}$, $^{18}\text{O}+^{208}\text{Pb}$, $^{32,36}\text{S}+^{90}\text{Zr}$, $^{34}\text{S}+^{168}\text{Er}$, $^{36}\text{S}+^{90,96}\text{Zr}$, $^{58}\text{Ni} + ^{58}\text{Ni}$, and $^{64}\text{Ni} + ^{58}\text{Ni}$, where there are no neutron transfer channels with positive Q -values, we extract the ground-state quadrupole deformation parameters $\beta_2=-0.3, 0.1, 0.312, 0.1, 0, 0.05$, and 0.087 , for the nuclei ^{12}C , ^{18}O , ^{32}S , ^{34}S , ^{36}S , ^{58}Ni , and ^{64}Ni , respectively, which are used in our calculations.

A. Role of neutron transfer in capture process at sub-barrier energies

After the neutron transfer in the reaction $^{40}\text{Ca}(\beta_2 = 0) + ^{96}\text{Zr}(\beta_2 = 0.08) \rightarrow ^{42}\text{Ca}(\beta_2 = 0.247) + ^{94}\text{Zr}(\beta_2 = 0.09)$ (Fig. 1) or $^{40}\text{Ca}(\beta_2 = 0) + ^{124}\text{Sn}(\beta_2 = 0.095) \rightarrow ^{42}\text{Ca}(\beta_2 = 0.247) + ^{122}\text{Sn}(\beta_2 = 0.1)$ (Fig. 1) the deformation of the nuclei increases and the mass asymmetry of the system decreases, and, thus, the value of the Coulomb barrier decreases and the capture cross section becomes larger (Fig. 1). In Fig. 2, we observe the same behavior in the reactions $^{58}\text{Ni}(\beta_2 = 0.05) + ^{132}\text{Sn}(\beta_2 = 0) \rightarrow ^{60}\text{Ni}(\beta_2 = 0.207) + ^{130}\text{Sn}(\beta_2 = 0)$ ($Q_{2n} = 7.8$ MeV), $^{58}\text{Ni}(\beta_2 = 0.05) + ^{130}\text{Te}(\beta_2 = 0) \rightarrow ^{60}\text{Ni}(\beta_2 = 0.207) + ^{128}\text{Te}(\beta_2 = 0)$ ($Q_{2n} = 5.9$ MeV), $^{64}\text{Ni}(\beta_2 = 0.087) + ^{132}\text{Sn}(\beta_2 = 0) \rightarrow ^{66}\text{Ni}(\beta_2 = 0.158) + ^{130}\text{Sn}(\beta_2 = 0)$ ($Q_{2n} = 2.5$ MeV), and $^{64}\text{Ni}(\beta_2 = 0.087) + ^{130}\text{Te}(\beta_2 = 0) \rightarrow ^{66}\text{Ni}(\beta_2 = 0.158) + ^{128}\text{Te}(\beta_2 = 0)$ ($Q_{2n} = 0.55$ MeV). One can see a good agreement between the calculated results and the experimental data [11–13]. So, the observed capture enhancement at sub-barrier energies in the reactions mentioned above is related to the two-neutron transfer channel. One can see that at energies above and near the Coulomb barrier the cross sections with and without two-neutron transfer are almost similar. Since the two-neutron transfer causes a larger change of the deformations of the nuclei in the reactions $^{58}\text{Ni} + ^{132}\text{Sn}, ^{130}\text{Te}$ than in the reactions $^{64}\text{Ni} + ^{132}\text{Sn}, ^{130}\text{Te}$, at sub-barrier energies the capture enhancement in the reactions with ^{58}Ni is larger than in the reactions with ^{64}Ni (Fig. 2).

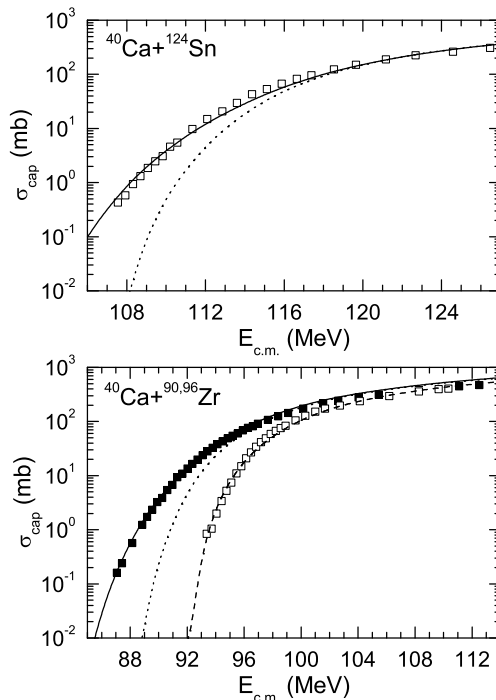


FIG. 1: The calculated capture cross sections versus $E_{c.m.}$ for the indicated reactions $^{40}\text{Ca} + ^{96}\text{Zr}$ (solid line), $^{40}\text{Ca} + ^{90}\text{Zr}$ (dashed line), and $^{48}\text{Ca} + ^{124}\text{Sn}$ (solid line). For the reactions $^{40}\text{Ca} + ^{96}\text{Zr}$, ^{124}Sn , the calculated capture cross sections without the neutron transfer process are shown by dotted lines. The experimental data (symbols) are from Refs. [11, 12].

One can make unambiguous statements regarding the neutron transfer process with a positive Q -value when the colliding nuclei are double magic or semi-magic. In this case one can disregard the deformation and orientation effects before the neutron transfer. To eliminate the influence of the nucleus-nucleus potential on the capture (fusion) cross section and to make conclusions about the role of deformation of colliding nuclei and the nucleon transfer between interacting nuclei in the capture (fusion) cross section, a reduction procedure is useful [15]. It consists of the following transformations:

$$E_{c.m.} \rightarrow x = \frac{E_{c.m.} - V_b}{\hbar\omega_b}, \quad \sigma_{cap} \rightarrow \sigma_{cap}^{red} = \frac{2E_{c.m.}}{\hbar\omega_b R_b^2} \sigma_{cap},$$

where $\sigma_{cap} = \sigma_{cap}(E_{c.m.})$ is the capture cross section at bombarding energy $E_{c.m.}$. The frequency $\omega_b = \sqrt{V''(R_b)}/\mu$ is related with the second derivative $V''(R_b)$ of the total nucleus-nucleus potential $V(R)$ (the Coulomb + nuclear parts) at the barrier position R_b . With these replacements we compared the reduced calculated capture (fusion) cross sections σ_{cap}^{red} for the reactions $^{40,48}\text{Ca} + ^{124,132}\text{Sn}$ (Fig. 3). The choice of the projectile-target combination is crucial, and for the systems studied one can make unambiguous statements regarding the neutron transfer process with a positive Q -value when the interacting nuclei are double magic or semi-magic spherical nuclei. In this case one can disregard the strong direct nuclear deformation effects. In Fig. 3, one can see that the reduced capture cross sections in the reactions $^{40}\text{Ca} + ^{124,132}\text{Sn}$ with the positive Q_{2n} -values strongly deviate from those in the reactions $^{48}\text{Ca} + ^{124,132}\text{Sn}$, where the neutron transfers are suppressed because of the negative Q -values. After two-neutron transfer in the reactions $^{40}\text{Ca}(\beta_2 = 0) + ^{124}\text{Sn}(\beta_2 = 0.1) \rightarrow ^{42}\text{Ca}(\beta_2 = 0.25) + ^{122}\text{Sn}(\beta_2 = 0.1)$ ($Q_{2n} = 5.4$ MeV) and $^{40}\text{Ca}(\beta_2 = 0) + ^{132}\text{Sn}(\beta_2 = 0) \rightarrow ^{42}\text{Ca}(\beta_2 = 0.25) + ^{130}\text{Sn}(\beta_2 = 0)$ ($Q_{2n} = 7.3$ MeV) the deformation of the light nucleus increases and the mass asymmetry of the system decreases and, thus, the value of the Coulomb barrier decreases and the capture cross section becomes larger (Fig. 3). So, because of the transfer effect the systems $^{40}\text{Ca} + ^{124,132}\text{Sn}$ show large sub-barrier enhancements with respect to the systems $^{48}\text{Ca} + ^{124,132}\text{Sn}$. We observe that the σ_{cap}^{red} in the $^{40}\text{Ca} + ^{124}\text{Sn}$ ($^{48}\text{Ca} + ^{124}\text{Sn}$) reaction are larger than those in the $^{40}\text{Ca} + ^{132}\text{Sn}$ ($^{48}\text{Ca} + ^{132}\text{Sn}$) reaction. The reason of that is the nonzero quadrupole deformation of the heavy nucleus ^{124}Sn . It should be stressed that there are almost no difference between σ_{cap}^{red} in the reactions $^{40,48}\text{Ca} + ^{124,132}\text{Sn}$ at energies above the Coulomb barrier.

In Figs. 4 and 5 one can see a good agreement between the calculated results and the experimental data in the reactions $^{40,48}\text{Ca} + ^{124,132}\text{Sn}$. This means that the observed capture enhancements in the reactions $^{40}\text{Ca} + ^{124,132}\text{Sn}$ at sub-barrier energies are related to the two-neutron transfer effect. Note that the slope of the excitation function

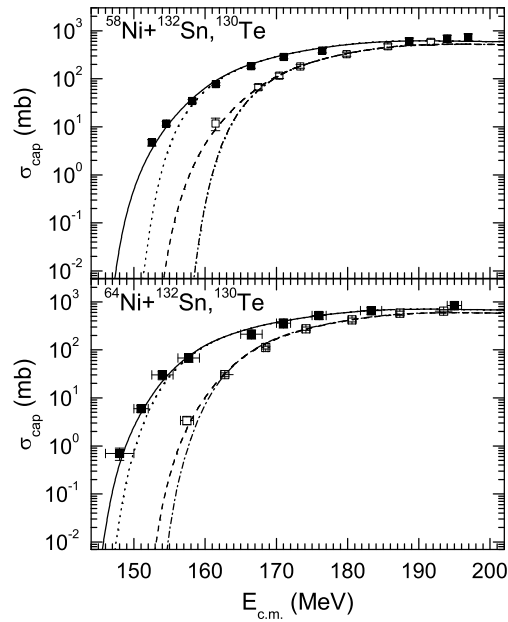


FIG. 2: The same as in Fig. 1, for the reactions $^{58,64}\text{Ni} + ^{132}\text{Sn}$ (solid lines) and $^{58,64}\text{Ni} + ^{130}\text{Te}$ (dashed lines). The experimental data (symbols) are from Refs. [13, 14]. For the reactions $^{58,64}\text{Ni} + ^{132}\text{Sn}$ (dotted lines) and $^{58,64}\text{Ni} + ^{130}\text{Te}$ (dash-dotted lines), the calculated capture cross sections without the neutron transfer are shown.

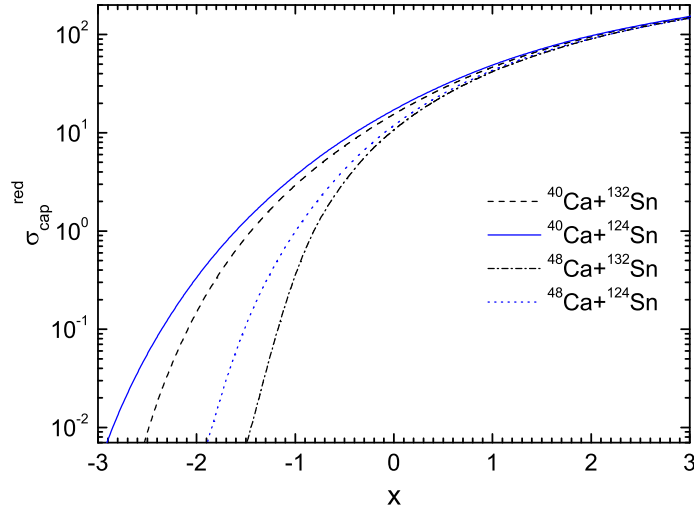


FIG. 3: (Color online) The calculated reduced capture cross sections versus $(E_{c.m.} - V_b)/(\hbar\omega_b)$ in the reactions $^{40}\text{Ca} + ^{124}\text{Sn}$ (solid line), $^{48}\text{Ca} + ^{124}\text{Sn}$ (dashed line), $^{48}\text{Ca} + ^{124}\text{Sn}$ (dotted line), and $^{48}\text{Ca} + ^{132}\text{Sn}$ (dash-dotted line).

strongly depends on the deformations of the interacting nuclei and, respectively, on the neutron transfer effect.

To describe the reactions $^{40,48}\text{Ca} + ^{132}\text{Sn}$ and $^{48}\text{Ca} + ^{124,132}\text{Sn}$ (Figs. 4 and 5), we extracted the values of the corresponding Coulomb barrier V_b for the spherical nuclei. There are differences between the calculated and extracted V_b . From the direct calculations of the nucleus-nucleus potentials (with the same set of parameters), we obtained $V_b(^{40}\text{Ca} + ^{124}\text{Sn}) - V_b(^{48}\text{Ca} + ^{124}\text{Sn}) = 2.3$ MeV, $V_b(^{40}\text{Ca} + ^{132}\text{Sn}) - V_b(^{48}\text{Ca} + ^{132}\text{Sn}) = 2.2$ MeV, $V_b(^{40}\text{Ca} + ^{124}\text{Sn}) - V_b(^{40}\text{Ca} + ^{132}\text{Sn}) = 1.3$ MeV, and $V_b(^{48}\text{Ca} + ^{124}\text{Sn}) - V_b(^{48}\text{Ca} + ^{132}\text{Sn}) = 1.2$ MeV. From the extractions, we got $V_b(^{40}\text{Ca} + ^{124}\text{Sn}) - V_b(^{48}\text{Ca} + ^{124}\text{Sn}) = 1.1$ MeV, $V_b(^{40}\text{Ca} + ^{132}\text{Sn}) - V_b(^{48}\text{Ca} + ^{132}\text{Sn}) = 1.0$ MeV, $V_b(^{40}\text{Ca} + ^{124}\text{Sn}) - V_b(^{40}\text{Ca} + ^{132}\text{Sn}) = -0.3$ MeV, and $V_b(^{48}\text{Ca} + ^{124}\text{Sn}) - V_b(^{48}\text{Ca} + ^{132}\text{Sn}) = -0.4$ MeV, which seem to be unrealistically small. However, these differences of V_b do not influence the slopes of the excitation functions but only lead to the shifting of the energy scale. With realistic isospin trend of V_b $\sigma_{cap}(^{40}\text{Ca} + ^{124}\text{Sn}) < \sigma_{cap}(^{48}\text{Ca} + ^{124}\text{Sn})$ and $\sigma_{cap}(^{40}\text{Ca} + ^{132}\text{Sn}) < \sigma_{cap}(^{48}\text{Ca} + ^{132}\text{Sn})$ at energies above the corresponding Coulomb barriers.

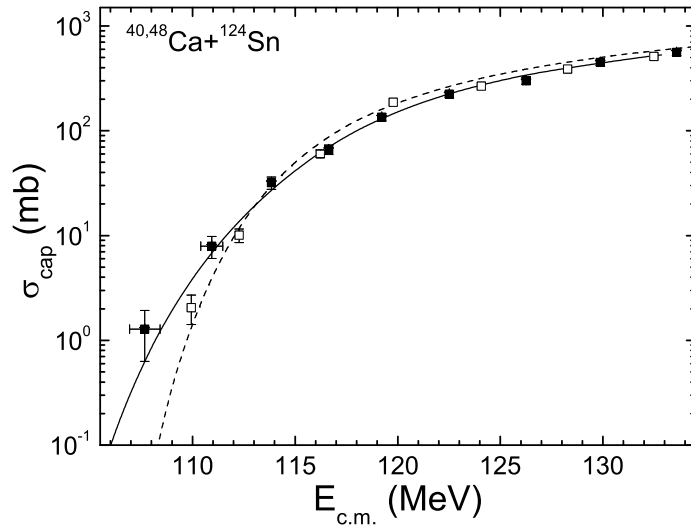


FIG. 4: (Color online) The calculated capture cross sections versus $E_{c.m.}$ for the reactions $^{40}\text{Ca}+^{124}\text{Sn}$ (solid line) and $^{48}\text{Ca}+^{124}\text{Sn}$ (dashed line). The experimental data for the reactions $^{40}\text{Ca}+^{124}\text{Sn}$ (solid squares) and $^{48}\text{Ca}+^{124}\text{Sn}$ (open squares) are from Ref. [16]. In the calculations the barriers were adjusted to the experimental values.

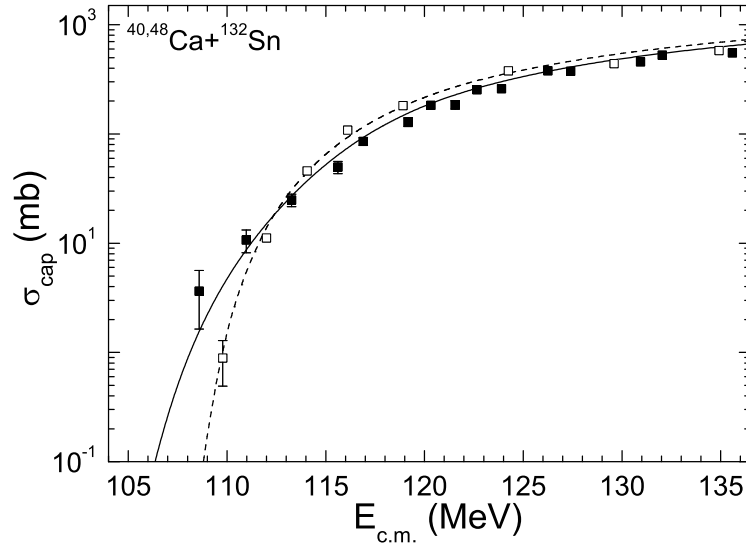


FIG. 5: (Color online) The calculated capture cross sections versus $E_{c.m.}$ for the reactions $^{40}\text{Ca}+^{132}\text{Sn}$ (solid line) and $^{48}\text{Ca}+^{132}\text{Sn}$ (dashed line). The experimental data for the reactions $^{40}\text{Ca}+^{132}\text{Sn}$ (solid squares) and $^{48}\text{Ca}+^{132}\text{Sn}$ (open squares) are from Ref. [16]. In the calculations the barriers were adjusted to the experimental values.

One can find reactions with a positive Q -values of the two-neutron transfer where the transfer weakly influences or even suppresses the capture process. This happens if after the transfer the deformations of the nuclei do not change much or even decrease. For instance, in the reactions $^{60}\text{Ni}(\beta_2 \approx 0.1) + ^{100}\text{Mo}(\beta_2 = 0.231) \rightarrow ^{62}\text{Ni}(\beta_2 = 0.198) + ^{98}\text{Mo}(\beta_2 = 0.168)$ ($Q_{2n} = 4.2$ MeV), $^{64}\text{Ni}(\beta_2 \approx 0.087) + ^{100}\text{Mo}(\beta_2 = 0.231) \rightarrow ^{66}\text{Ni}(\beta_2 = 0.158) + ^{98}\text{Mo}(\beta_2 = 0.168)$ ($Q_{2n} = 0.94$ MeV), and $^{60}\text{Ni}(\beta_2 \approx 0.1) + ^{150}\text{Nd}(\beta_2 = 0.285) \rightarrow ^{62}\text{Ni}(\beta_2 = 0.198) + ^{148}\text{Nd}(\beta_2 = 0.204)$ ($Q_{2n} = 6$ MeV) we expect a weak dependence of the capture cross section on the neutron transfer (Fig. 6). There is the experimental evidence [17] of such an effect for the $^{60}\text{Ni} + ^{100}\text{Mo}$ reaction. So, the two-neutron transfer channel with large positive Q_{2n} -value weakly influences the fusion (capture) cross section. The reduced capture cross sections in the reactions $^{60}\text{Ni} + ^{100}\text{Mo}, ^{150}\text{Nd}$ are close to each other in contrast to those in the reactions $^{58,64}\text{Ni} + ^{132}\text{Sn}, ^{130}\text{Te}$. The $^{60}\text{Ni} + ^{150}\text{Nd}$ reaction has even a small suppression due to the neutron transfer.

Figures 7-9 show the capture excitation function for the reactions $^{32,36}\text{S}+\text{Pd,Ru}$ as a function of the bombarding energy. One can see a relatively good agreement between the calculated results and the experimental data [18]. The

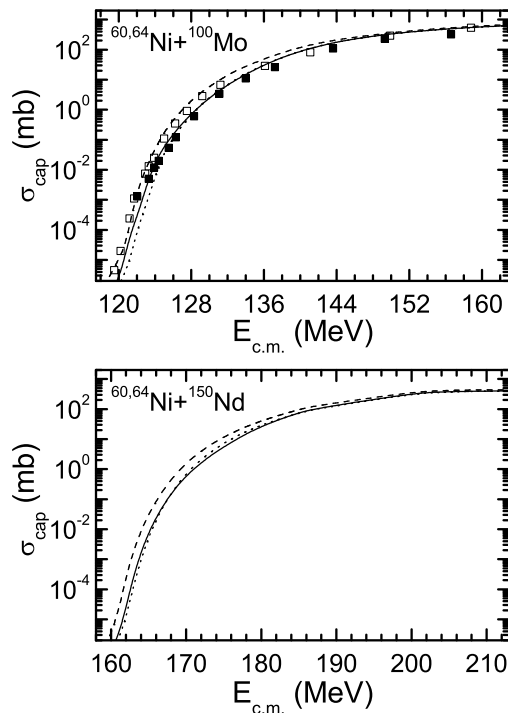


FIG. 6: (Color online) The same as in Fig. 1, for the indicated reactions $^{60}\text{Ni} + ^{100}\text{Mo}$, ^{150}Nd (solid lines), and $^{64}\text{Ni} + ^{100}\text{Mo}$, ^{150}Nd (dashed lines). For the reactions $^{60}\text{Ni} + ^{100}\text{Mo}$ and $^{60}\text{Ni} + ^{150}\text{Nd}$, the calculated capture cross sections without the neutron transfer are shown by dotted lines. The experimental data for the reactions $^{60}\text{Ni} + ^{100}\text{Mo}$ (closed squares) and $^{64}\text{Ni} + ^{100}\text{Mo}$ (open squares) are from Ref. [17].

Q_{2n} -values for the $2n$ -transfer processes are positive (negative) for all reactions with ^{32}S (^{36}S). At energies above and near the Coulomb barrier the cross sections with and without two-neutron transfer are almost similar. After the $2n$ -transfer (before the capture) in the reactions $^{32}\text{S}(\beta_2 = 0.312) + ^{110}\text{Pd}(\beta_2 = 0.257) \rightarrow ^{34}\text{S}(\beta_2 = 0.252) + ^{108}\text{Pd}(\beta_2 = 0.243)$, $^{32}\text{S}(\beta_2 = 0.312) + ^{108}\text{Pd}(\beta_2 = 0.243) \rightarrow ^{34}\text{S}(\beta_2 = 0.252) + ^{106}\text{Pd}(\beta_2 = 0.229)$, $^{32}\text{S}(\beta_2 = 0.312) + ^{106}\text{Pd}(\beta_2 = 0.229) \rightarrow ^{34}\text{S}(\beta_2 = 0.252) + ^{104}\text{Pd}(\beta_2 = 0.209)$, $^{32}\text{S}(\beta_2 = 0.312) + ^{104}\text{Pd}(\beta_2 = 0.209) \rightarrow ^{34}\text{S}(\beta_2 = 0.252) + ^{102}\text{Pd}(\beta_2 = 0.196)$, or $^{32}\text{S}(\beta_2 = 0.312) + ^{104}\text{Ru}(\beta_2 = 0.271) \rightarrow ^{34}\text{S}(\beta_2 = 0.252) + ^{102}\text{Ru}(\beta_2 = 0.24)$, $^{32}\text{S}(\beta_2 = 0.312) + ^{102}\text{Ru}(\beta_2 = 0.24) \rightarrow ^{34}\text{S}(\beta_2 = 0.252) + ^{100}\text{Ru}(\beta_2 = 0.215)$, $^{32}\text{S}(\beta_2 = 0.312) + ^{100}\text{Ru}(\beta_2 = 0.215) \rightarrow ^{34}\text{S}(\beta_2 = 0.252) + ^{98}\text{Ru}(\beta_2 = 0.195)$ the deformations of the nuclei decrease and the values of the corresponding Coulomb barriers increase. As a result, the transfer suppresses the capture process in these reactions at the sub-barrier energies. The suppression becomes stronger with decreasing energy (Figs. 7-9). As seen in Fig. 7, the capture cross sections calculated without two-neutron transfer are larger than those calculated with two-neutron transfer in the case of the $^{32}\text{S} + ^{110}\text{Pd}$ reaction. The enhancement of the sub-barrier fusion for the reactions with ^{32}S with respect to the reactions with ^{36}S is related to a larger deformation of ^{34}S in comparison with ^{36}S . We observe the same behavior in the reactions $^{32,36}\text{S} + ^{94,96,98,100}\text{Mo}$.

Figures 10 and 11 show the excitation functions for the reactions $^{18}\text{O} + ^{74}\text{Ge}$, $^{112,118,124}\text{Sn}$ and $^{32}\text{S} + ^{112,116}\text{Sn}$. For the ^{32}S -induced reactions, $Q_{2n} > 0$. For the projectile ^{18}O there is a large range of positive Q_{2n} -values, for example, varying from 1.4 MeV for $^{18}\text{O} + ^{124}\text{Sn}$ up to 5.5 MeV for $^{18}\text{O} + ^{112}\text{Sn}$. The agreement between the calculated results and the experimental data [20, 22] is rather good. As seen in Fig. 11, the cross sections increase systematically with the target mass number and run nearly similarly down to the lowest energy treated. In the reactions $^{32}\text{S}(\beta_2 = 0.312) + ^{112}\text{Sn}(\beta_2 = 0.123) \rightarrow ^{34}\text{S}(\beta_2 = 0.252) + ^{110}\text{Sn}(\beta_2 = 0.122)$, $^{32}\text{S}(\beta_2 = 0.312) + ^{116}\text{Sn}(\beta_2 = 0.112) \rightarrow ^{34}\text{S}(\beta_2 = 0.252) + ^{114}\text{Sn}(\beta_2 = 0.121)$, $^{18}\text{O}(\beta_2 = 0.1) + ^{74}\text{Ge}(\beta_2 = 0.283) \rightarrow ^{16}\text{O}(\beta_2 = 0) + ^{76}\text{Ge}(\beta_2 = 0.262)$, $^{18}\text{O}(\beta_2 = 0.1) + ^{112}\text{Sn}(\beta_2 = 0.123) \rightarrow ^{16}\text{O}(\beta_2 = 0) + ^{114}\text{Sn}(\beta_2 = 0.121)$, $^{18}\text{O}(\beta_2 = 0.1) + ^{118}\text{Sn}(\beta_2 = 0.111) \rightarrow ^{16}\text{O}(\beta_2 = 0) + ^{120}\text{Sn}(\beta_2 = 0.104)$, and $^{18}\text{O}(\beta_2 = 0.1) + ^{124}\text{Sn}(\beta_2 = 0.095) \rightarrow ^{16}\text{O}(\beta_2 = 0) + ^{126}\text{Sn}(\beta_2 = 0.09)$ the $2n$ -transfer suppresses the capture process (Figs. 10 and 11). The sub-barrier capture cross sections for the systems $^{18}\text{O} + ^A\text{Sn}$ studied here do not show any strong dependence on the mass number of the target isotope. Our results show that cross sections for reactions $^{16}\text{O} + ^{76}\text{Ge}$ ($^{16}\text{O} + ^{114,120,126}\text{Sn}$) [$Q_{2n} < 0$] and $^{18}\text{O} + ^{74}\text{Ge}$ ($^{18}\text{O} + ^{112,118,124}\text{Sn}$) are very similar (Fig. 10). Just the same behavior was observed in the recent experiments $^{16,18}\text{O} + ^{76,74}\text{Ge}$ [20].

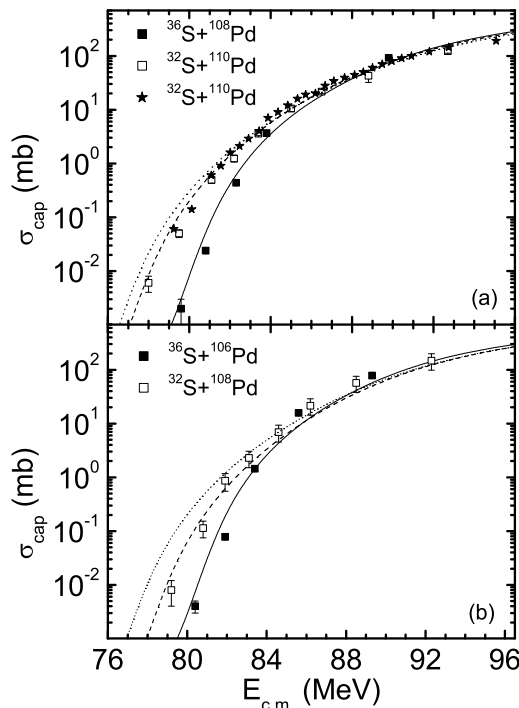


FIG. 7: The calculated capture cross sections vs $E_{c.m.}$ for the reactions $^{32}\text{S}+^{108,110}\text{Pd}$ (dashed lines) and $^{36}\text{S}+^{106,108}\text{Pd}$ (solid lines) (a,b). For the $^{32}\text{S}+^{110}\text{Pd}$ reaction (a), the calculated capture cross section without the neutron transfer process is shown by a dotted line. For the reactions $^{32}\text{S}+^{110}\text{Pd}$, the experimental data from [18] and [19] are marked by open squares and stars, respectively.

B. Neutron transfer in reactions with weakly bound nuclei

After the neutron transfer in the reactions $^{13}\text{C}+^{232}\text{Th}(\beta_2 = 0.261) \rightarrow ^{14}\text{C}(\beta_2 = -0.36) + ^{231}\text{Th}(\beta_2 = 0.261)$ ($Q_{1n} = 1.74$ MeV), $^{15}\text{C}+^{232}\text{Th}(\beta_2 = 0.261) \rightarrow ^{14}\text{C}(\beta_2 = -0.36) + ^{233}\text{Th}(\beta_2 = 0.261)$ ($Q_{1n} = 3.57$ MeV) the deformations of the target or projectile nuclei in these reactions and in the $^{14}\text{C}+^{232}\text{Th}(\beta_2 = 0.261)$ ($Q_{1n,2n} < 0$) reaction are the same. In Fig. 12 the calculated cross sections slightly increase with the mass number of C, and are nearly parallel down to the lowest energy treated. There is a relatively good agreement between the calculated results [6] and the experimental data [24, 25] for the reactions $^{12,13,14}\text{C}+^{232}\text{Th}$, but the experimental enhancement of the cross section in the $^{15}\text{C}+^{232}\text{Th}$ reaction at sub-barrier energies cannot be explained with our and other [24] models. Because we take into account the neutron transfer ($^{15}\text{C} \rightarrow ^{14}\text{C}$), one can suppose that this discrepancy is attributed to the influence of the breakup channel [1] which is not considered in our model. However, it is unclear why the breakup process influences only two experimental points at lowest energies. Different deviations of these points in energy from the calculated curve in Fig. 12 create doubt in an influence of the breakup on the kinetic energy. So, additional experimental and theoretical investigations are desirable.

The question is whether the fusion of nuclei involving weakly bound neutrons is enhanced or suppressed at low energies. This question can be addressed to the systems $^{12-15}\text{C}+^{208}\text{Pb}$ [26]. After the neutron transfer in the reactions $^{13}\text{C}+^{208}\text{Pb}(\beta_2 = 0) \rightarrow ^{14}\text{C}(\beta_2 = -0.36) + ^{207}\text{Pb}(\beta_2 = 0)$ ($Q_{1n} = 1.74$ MeV), $^{15}\text{C}+^{208}\text{Pb}(\beta_2 = 0) \rightarrow ^{14}\text{C}(\beta_2 = -0.36) + ^{209}\text{Pb}(\beta_2 = 0.055)$ ($Q_{1n} = 3.57$ MeV) the deformations of the light nuclei are the same as in the $^{14}\text{C}+^{208}\text{Pb}(\beta_2 = 0)$ ($Q_{1n,2n} < 0$) reaction. The heavy nuclei are almost spherical. This means that the slopes of the excitation functions are almost the same (Fig. 13). As in the case of the $^{15}\text{C}+^{232}\text{Th}$ reaction, we do not expect enhancement of the capture cross section in the $^{15}\text{C}+^{208}\text{Pb}$ reaction owing to the neutron transfer. The same effect was observed in Ref. [26]. The study of the reactions $^{15}\text{C}+^{208}\text{Pb}, ^{232}\text{Th}$ at sub-barrier energies provides a good test for the verification of the effect of weakly bound nuclei on fusion and capture because it reveals the role of other effects besides neutron transfer.

By assuming that the $2n$ -transfer process takes place and the break-up channels are closed, one can predict almost the same capture cross sections for the reaction with large positive Q_{2n} value $^6\text{He}+^{206}\text{Pb}$ ($^9\text{Li}+^{68}\text{Zn}$) and for the complemented reaction $^4\text{He}+^{208}\text{Pb}$ ($^7\text{Li}+^{70}\text{Zn}$). Indeed, after the transfer in the reactions $^6\text{He}+^{206}\text{Pb} \rightarrow ^4\text{He}(\beta_2 = 0) + ^{208}\text{Pb}(\beta_2 = 0.055)$ ($Q_{2n} = 13.13$ MeV), $^9\text{Li}+^{86}\text{Zn} \rightarrow ^7\text{Li}(\beta_2 \approx 0.4) + ^{70}\text{Zn}(\beta_2 = 0.248)$ ($Q_{2n} = 9.60$ MeV) they

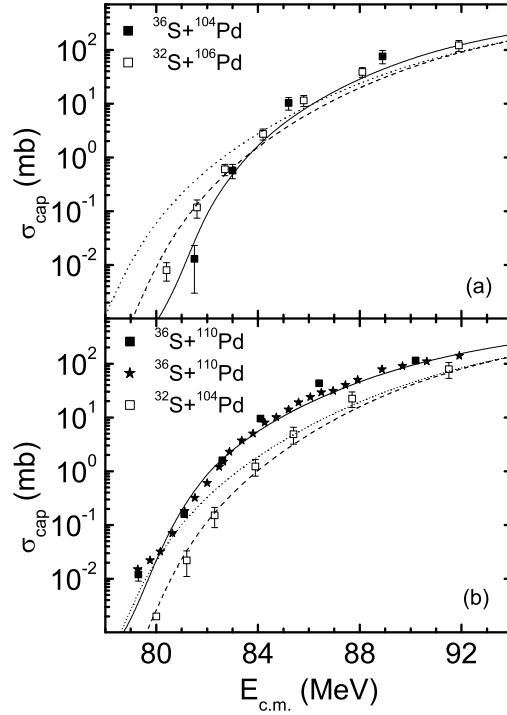


FIG. 8: The same as in Fig. 7, for the reactions $^{32}\text{S}+^{104,106}\text{Pd}$ (dashed lines) and $^{36}\text{S}+^{104,110}\text{Pd}$ (solid lines) (a,b). The dotted lines correspond to the reactions $^{32}\text{S}+^{104,106}\text{Pd}$ when the neutron transfer is disregarded. The experimental data (symbols) are from Ref. [18].

become equivalent to the reactions $^4\text{He}+^{208}\text{Pb}$ and $^7\text{Li}+^{70}\text{Zn}$. Therefore, the slopes of the excitation functions in the reactions with ^6He (^9Li) and ^4He (^7Li) should be similar. This conclusion supports the experimental data of Ref. [28], where the authors concluded that the fusion enhancement in the $^6\text{He}+^{206}\text{Pb}$ reaction (with respect to the $^4\text{He}+^{208}\text{Pb}$ reaction) is rather small or absent.

By assuming that the $2n$ -transfer process occurs, we calculated the capture cross sections for the $^9\text{Li}+^{70}\text{Zn}$ reaction (Fig. 14). The agreement with the experimental data of Ref. [29] is quite satisfactory. At lowest energies, the calculated cross section is by factor of ~ 5 less than the experimental value. The experimental data are well reproduced by the model [30] where two-neutron transfer from the ^{70}Zn leads to ^{11}Li halo structure and molecular bond between the nuclei in contact enhances the fusion cross section. Note that two-neutron transfer $^9\text{Li}+^{70}\text{Zn}\rightarrow^7\text{Li}+^{72}\text{Zn}$ with $Q_{2n} = 8.6$ MeV is much energetically favorable than the two-neutron transfer $^9\text{Li}+^{70}\text{Zn}\rightarrow^{11}\text{Li}+^{68}\text{Zn}$ with $Q_{2n} = -15.4$ MeV. These observations deserve further experimental and theoretical investigations including the breakup channel.

C. Breakup probabilities

The difference between the calculated capture cross section σ_{cap}^{th} in the absence of breakup and the experimental complete fusion cross section σ_{fus}^{exp} can be ascribed to the breakup effect with the probability [31]

$$P_{BU} = 1 - \sigma_{fus}^{exp}/\sigma_c^{th}. \quad (3)$$

If at some energy $\sigma_{fus}^{exp} > \sigma_{cap}^{th}$, the values of σ_{cap}^{th} was normalized so to have $P_{BU} \geq 0$ at any energy. Note that $\sigma_{fus}^{exp} = \sigma_{fus}^{noBU} + \sigma_{fus}^{BU}$ contains the contribution from two processes: the direct fusion of the projectile with the target (σ_{fus}^{noBU}), and the breakup of the projectile followed by the fusion of the two projectile fragments with the target (σ_{fus}^{BU}). A more adequate estimate of the breakup probability would then be:

$$P_{BU} = 1 - \sigma_{fus}^{noBU}/\sigma_{cap}^{th}, \quad (4)$$

which leads to larger values of P_{BU} than the expression employed by us. However, the ratio between σ_{fus}^{noBU} and σ_{fus}^{BU} cannot be measured experimentally but can be estimated with the approach suggested in Ref. [32]. The parameters

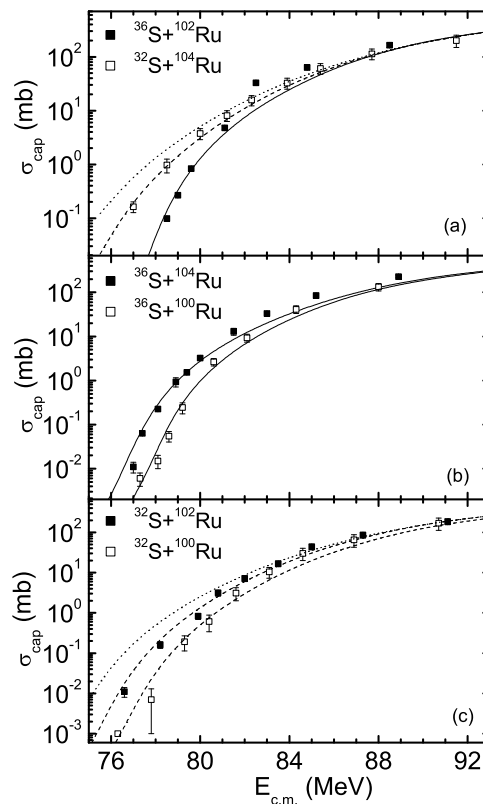


FIG. 9: The calculated capture cross sections vs $E_{c.m.}$ for the reactions $^{36}\text{S}+^{100,102,104}\text{Ru}$ (dashed lines) (a,b,c) and $^{36}\text{S}+^{100,102,104}\text{Ru}$ (solid lines) (a,b). The dotted lines correspond to the reactions $^{32}\text{S}+^{102,104}\text{Ru}$ (a,c) when the neutron transfer is disregarded. The experimental data (symbols) are from Ref. [18].

of the potential are taken to fit the height of the Coulomb barrier obtained in our calculations. The parameters of the breakup function [32] are set to describe the value of σ_{fus}^{exp} . As shown in Ref. [32] and in our calculations, in the $^8\text{Be}+^{208}\text{Pb}$ reaction the fraction of σ_{fus}^{BU} in σ_{fus}^{exp} does not exceed few percents at $E_{c.m.} - V_b < 4$ MeV. This fraction rapidly increases and reaches about 12–20%, depending on the reaction, at $E_{c.m.} - V_b \approx 10$ MeV. Because we are mainly interested in the energies near and below the barrier, the estimated σ_{fus}^{BU} does not exceed 20% of σ_{fus}^{exp} at $E_{c.m.} - V_b < 10$ MeV. The results for P_{BU} are presented, taking σ_{fus}^{noBU} into account in Eq. (4).

As seen in Figs. 15 and 16, at energies above the Coulomb barriers the values of P_{BU} vary from 0 to 84%. In the reactions $^9\text{Be}+^{144}\text{Sm}, ^{208}\text{Pb}, ^{209}\text{Bi}$ the value of P_{BU} increases with charge number of the target at $E_{c.m.} - V_b > 3$ MeV. This was also noted in Ref. [33]. However, the reactions $^9\text{Be}+^{89}\text{Y}, ^{124}\text{Sn}$ are out of this systematics. In the reactions $^6\text{Li}+^{144}\text{Sm}, ^{198}\text{Pt}, ^{209}\text{Bi}$ the value of P_{BU} decreases with increasing charge number of the target at $E_{c.m.} - V_b > 3$ MeV. While in the reactions $^9\text{Be}+^{89}\text{Y}, ^{144}\text{Sm}, ^{208}\text{Pb}, ^{209}\text{Bi}$ the value of P_{BU} has a minimum at $E_{c.m.} - V_b \approx 0$ and a maximum at $E_{c.m.} - V_b \approx -(1-3)$ MeV, in the $^9\text{Be}+^{124}\text{Sn}$ reaction the value of P_{BU} steadily decreases with energy. In the reactions $^6\text{Li}+^{144}\text{Sm}, ^{198}\text{Pt}, ^{209}\text{Bi}, ^7\text{Li}+^{208}\text{Pb}, ^{209}\text{Bi}$, and $^9\text{Li}+^{208}\text{Pb}$ there is maximum of P_{BU} at $E_{c.m.} - V_b \approx -(0-1)$ MeV. However, in the reactions $^6\text{Li}+^{208}\text{Pb}$ and $^7\text{Li}+^{165}\text{Ho}$ P_{BU} has a minima $E_{c.m.} - V_b \approx 2$ MeV and no maxima at $E_{c.m.} - V_b \approx 0$. For ^9Be , the breakup threshold is slightly larger than for ^6Li . Therefore, we cannot explain a larger breakup probability at smaller $E_{c.m.} - V_b$ in the case of ^9Be .

IV. QUASI-ELASTIC AND ELASTIC BACKSCATTERING - TOOLS FOR SEARCH OF BREAKUP PROCESS IN REACTIONS WITH WEAKLY BOUND PROJECTILES

The lack of a clear systematic behavior of the complete fusion suppression as a function of the target charge requires new additional experimental and theoretical studies. The quasi-elastic backscattering has been used [31, 34] as an alternative to investigate fusion (capture) barrier distributions, since this process is complementary to fusion. Since the quasi-elastic experiment is usually not as complex as the capture (fusion) and breakup measurements, they are well suited to survey the breakup probability. There is a direct relationship between the capture, the quasi-elastic

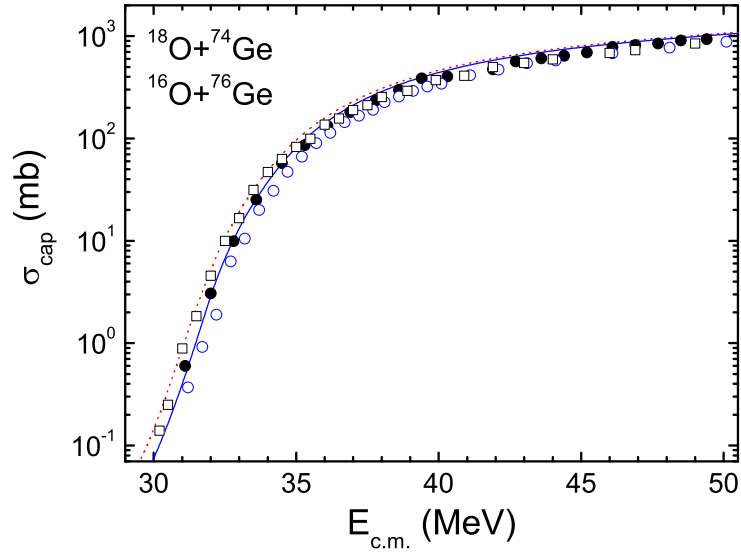


FIG. 10: (Color online) The calculated (solid line) capture cross sections vs $E_{c.m.}$ for the reactions $^{16}\text{O}+^{76}\text{Ge}$ and $^{18}\text{O}+^{74}\text{Ge}$ (the curves coincide). For the $^{18}\text{O}+^{74}\text{Ge}$ reaction, the calculated capture cross sections without neutron transfer are shown by dotted line. The experimental data for the reactions $^{16}\text{O}+^{76}\text{Ge}$ (open circles) and $^{18}\text{O}+^{74}\text{Ge}$ (open squares) are from Ref. [20]. The experimental data for the $^{16}\text{O}+^{76}\text{Ge}$ reaction (solid circles) are from Ref. [21].

scattering and the breakup processes, since any loss from the quasi-elastic and breakup channel contributes directly to capture (the conservation of the total reaction flux):

$$P_{qe}(E_{c.m.}, J) + P_{cap}(E_{c.m.}, J) + P_{BU}(E_{c.m.}, J) = 1, \quad (5)$$

where P_{qe} is the reflection quasi-elastic probability, P_{BU} is the breakup probability, and P_{cap} is the capture probability. The quasi-elastic scattering (P_{qe}) is the sum of all direct reactions, which include elastic (P_{el}), inelastic (P_{in}), and a few nucleon transfer (P_{tr}) processes. In Eq. (5) we neglect the deep inelastic collision process, since we are concerned with low energies. Equation (5) can be rewritten as

$$\frac{P_{qe}(E_{c.m.}, J)}{1 - P_{BU}(E_{c.m.}, J)} + \frac{P_{cap}(E_{c.m.}, J)}{1 - P_{BU}(E_{c.m.}, J)} = P_{qe}^{noBU}(E_{c.m.}, J) + P_{cap}^{noBU}(E_{c.m.}, J) = 1, \quad (6)$$

where

$$P_{qe}^{noBU}(E_{c.m.}, J) = \frac{P_{qe}(E_{c.m.}, J)}{1 - P_{BU}(E_{c.m.}, J)}$$

and

$$P_{cap}^{noBU}(E_{c.m.}, J) = \frac{P_{cap}(E_{c.m.}, J)}{1 - P_{BU}(E_{c.m.}, J)}$$

are the quasi-elastic and capture probabilities, respectively, in the absence of the breakup process. From these expressions we obtain the useful formulas

$$\frac{P_{qe}(E_{c.m.}, J)}{P_{cap}(E_{c.m.}, J)} = \frac{P_{qe}^{noBU}(E_{c.m.}, J)}{P_{cap}^{noBU}(E_{c.m.}, J)} = \frac{P_{qe}^{noBU}(E_{c.m.}, J)}{1 - P_{qe}^{noBU}(E_{c.m.}, J)} = a. \quad (7)$$

Using Eqs. (5) and (7), we obtain the relationship between breakup and quasi-elastic processes:

$$P_{BU}(E_{c.m.}, J) = 1 - P_{qe}(E_{c.m.}, J)[1 + 1/a] = 1 - \frac{P_{qe}(E_{c.m.}, J)}{P_{qe}^{noBU}(E_{c.m.}, J)}. \quad (8)$$

The reflection quasi-elastic probability $P_{qe}(E_{c.m.}, J = 0) = d\sigma_{qe}/d\sigma_{Ru}$ for bombarding energy $E_{c.m.}$ and angular momentum $J = 0$ is given by the ratio of the quasi-elastic differential cross section σ_{qe} and Rutherford differential

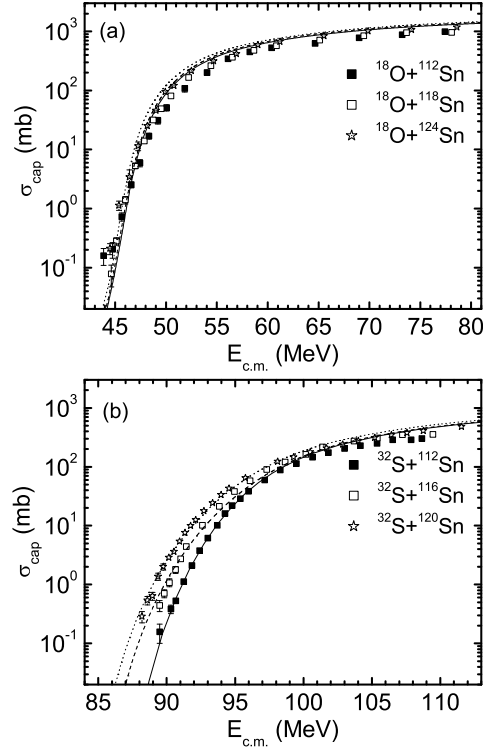


FIG. 11: The calculated capture cross sections vs $E_{c.m.}$ for the reactions $^{18}\text{S}+^{112,118,124}\text{Sn}$ (solid, dashed and dotted lines, respectively) (a) and $^{32}\text{S}+^{112,116,120}\text{Sn}$ (solid, dashed and dotted lines, respectively) (b). The experimental data (symbols) are from Ref. [22, 23].

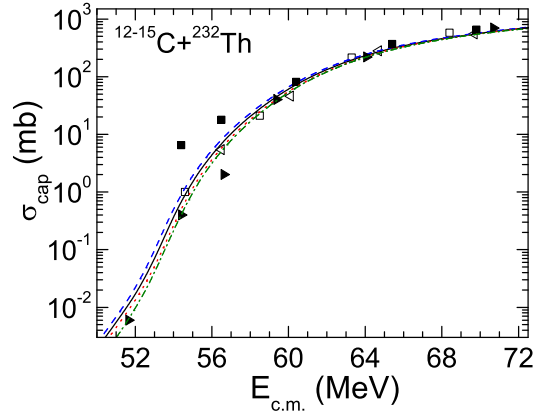


FIG. 12: (Color online) The calculated (lines) and experimental (symbols) capture cross sections vs $E_{c.m.}$ for the reactions $^{12}\text{C}+^{232}\text{Th}$ (dash-dotted line, solid triangles), $^{13}\text{C}+^{232}\text{Th}$ (dotted line, open triangles), $^{14}\text{C}+^{232}\text{Th}$ (solid line, open squares), and $^{15}\text{C}+^{232}\text{Th}$ (dashed line, solid squares). The experimental data are from Refs. [24, 25].

cross section σ_{Ru} at 180 degrees [34]. Employing Eq. (8) and the experimental quasi-elastic backscattering data with toughly and weakly bound isotopes-projectiles and the same compound nucleus, one can extract the breakup probability of the exotic nucleus. For example, using Eq. (8) at backward angle, the experimental $P_{qe}^{noBU}[{}^4\text{He}+{}^A\text{X}]$ of the ${}^4\text{He}+{}^A\text{X}$ reaction with toughly bound nuclei (without breakup), and $P_{qe}[{}^6\text{He}+{}^{A-2}\text{X}]$ of the ${}^6\text{He}+{}^{A-2}\text{X}$ reaction with weakly bound projectile (with breakup), and taking into consideration $V_b({}^4\text{He}+{}^A\text{X}) \approx V_b({}^6\text{He}+{}^{A-2}\text{X})$ for the very asymmetric systems, one can extract the breakup probability of the ${}^6\text{He}$:

$$P_{BU}(E_{c.m.}, J=0) = 1 - \frac{P_{qe}(E_{c.m.}, J=0)[{}^6\text{He}+{}^{A-2}\text{X}]}{P_{qe}^{noBU}(E_{c.m.}, J=0)[{}^4\text{He}+{}^A\text{X}]} \quad (9)$$

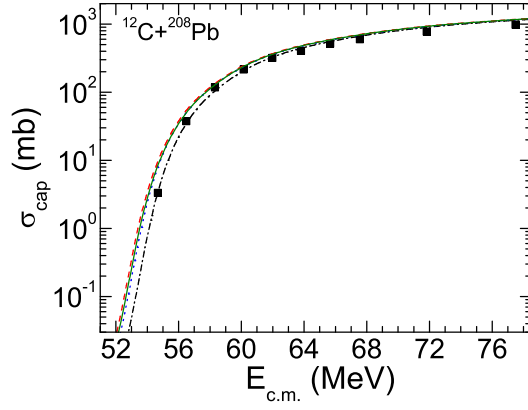


FIG. 13: The calculated (lines) and experimental (symbols) capture cross sections vs $E_{c.m.}$ for the reactions $^{12}\text{C}+^{208}\text{Pb}$ (dash-dotted line), $^{13}\text{C}+^{208}\text{Pb}$ (dotted line), $^{14}\text{C}+^{208}\text{Pb}$ (solid line), and $^{15}\text{C}+^{208}\text{Pb}$ (dashed line). The experimental data (solid squares) for the $^{12}\text{C}+^{208}\text{Pb}$ reaction are from Ref. [27].

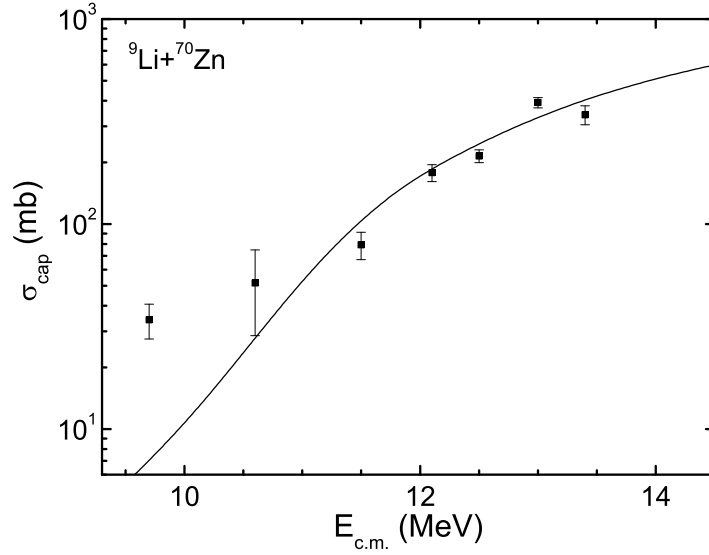


FIG. 14: The calculated (solid line) and experimental (symbols) capture cross sections vs $E_{c.m.}$ for the reaction $^9\text{Li}+^{70}\text{Zn}$. The experimental data are from Ref. [29].

Comparing the experimental quasi-elastic backscattering cross sections in the presence and absence of breakup data in the reaction pairs $^6\text{He}+^{68}\text{Zn}$ and $^4\text{He}+^{70}\text{Zn}$, $^6\text{He}+^{122}\text{Sn}$ and $^4\text{He}+^{124}\text{Sn}$, $^6\text{He}+^{236}\text{U}$ and $^4\text{He}+^{238}\text{U}$, $^8\text{He}+^{204}\text{Pb}$ and $^4\text{He}+^{208}\text{Pb}$, $^8\text{Li}+^{207}\text{Pb}$ and $^7\text{Li}+^{208}\text{Pb}$, $^7\text{Be}+^{207}\text{Pb}$ and $^{10}\text{Be}+^{204}\text{Pb}$, $^9\text{Be}+^{208}\text{Pb}$ and $^{10}\text{Be}+^{207}\text{Pb}$, $^{11}\text{Be}+^{206}\text{Pb}$ and $^{10}\text{Be}+^{207}\text{Pb}$, $^8\text{B}+^{208}\text{Pb}$ and $^{10}\text{B}+^{206}\text{Pb}$, $^8\text{B}+^{207}\text{Pb}$ and $^{11}\text{B}+^{204}\text{Pb}$, $^9\text{B}+^{208}\text{Pb}$ and $^{11}\text{B}+^{206}\text{Pb}$, $^{15}\text{C}+^{204}\text{Pb}$ and $^{12}\text{C}+^{207}\text{Pb}$, $^{15}\text{C}+^{206}\text{Pb}$ and $^{13}\text{C}+^{208}\text{Pb}$, $^{15}\text{C}+^{207}\text{Pb}$ and $^{14}\text{C}+^{208}\text{Pb}$, $^{17}\text{F}+^{206}\text{Pb}$ and $^{19}\text{F}+^{208}\text{Pb}$, leading to the same corresponding compound nuclei, one can analyze the role of the breakup channels in the reactions with the light weakly bound projectiles $^6,^8\text{He}$, ^8Li , $^{7,9,11}\text{Be}$, $^{8,9}\text{B}$, ^{15}C , and ^{17}F at near and above the barrier energies. On other side, the experimental uncertainties could be probably smaller when the same target-nucleus ^AX is used in the reactions with weakly and toughly bound isotopes. Then, one can extract the breakup probability of the ^6He [$\Delta E = V_b(^4\text{He} + ^A\text{X}) - V_b(^6\text{He} + ^A\text{X})$]:

$$P_{BU}(E_{c.m.}, J=0) = 1 - \frac{P_{qe}(E_{c.m.}, J=0)[^6\text{He} + ^A\text{X}]}{P_{qe}^{noBU}(E_{c.m.} + \Delta E, J=0)[^4\text{He} + ^A\text{X}]} \quad (10)$$

For the very asymmetric systems, one can neglect ΔE .

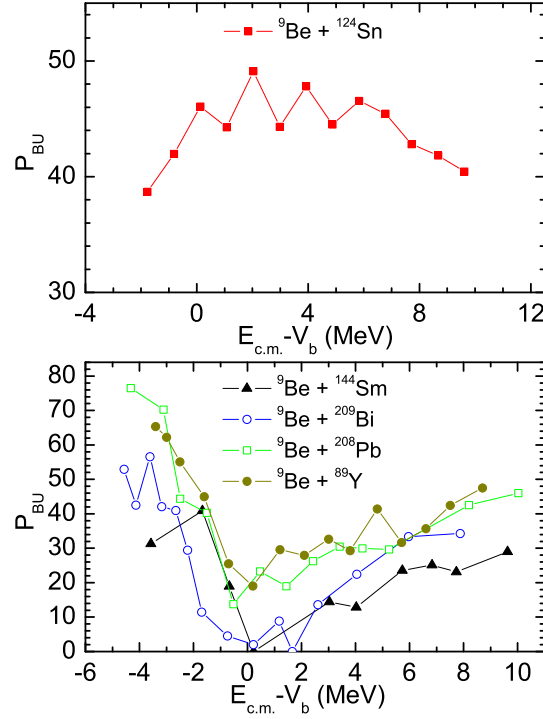


FIG. 15: (Color online) The dependence of the extracted breakup probability P_{BU} vs $E_{c.m.} - V_b$ for the indicated reactions with ${}^9\text{Be}$ -projectiles in %. Formula (4) was used.

Using the conservation of the total reaction flux, analogously one can find the following expression

$$P_{BU}(E_{c.m.}, J) = 1 - \frac{P_{el}(E_{c.m.}, J)}{P_{el}^{noBU}(E_{c.m.}, J)}, \quad (11)$$

which relates the breakup and elastic scattering processes. $P_{el}^{noBU}(E_{c.m.}, J)$ is the elastic scattering probability in the absence of the breakup process. So, one can extract the breakup probability of the ${}^6\text{He}$ at the backward angle:

$$P_{BU}(E_{c.m.}, J = 0) = 1 - \frac{P_{el}(E_{c.m.}, J = 0)[{}^6\text{He} + {}^{A-2}\text{X}]}{P_{el}^{noBU}(E_{c.m.}, J = 0)[{}^4\text{He} + {}^A\text{X}]} \quad (12)$$

or

$$P_{BU}(E_{c.m.}, J = 0) = 1 - \frac{P_{el}(E_{c.m.}, J = 0)[{}^6\text{He} + {}^A\text{X}]}{P_{el}^{noBU}(E_{c.m.} + \Delta E, J = 0)[{}^4\text{He} + {}^A\text{X}]}. \quad (13)$$

One concludes that the quasi-elastic or elastic backscattering technique could be a very important tool in breakup research. We propose to extract the breakup probability directly from the quasi-elastic or elastic backscattering probabilities of systems mentioned above.

V. SUMMARY

The quantum diffusion approach was applied to study the role of the neutron transfer with positive Q -value in the capture reactions at sub-, near- and above-barrier energies. We demonstrated a good agreement of the theoretical calculations with the experimental data. We found, that the change of the magnitude of the capture cross section after the neutron transfer occurs due to the change of the deformations of nuclei. The effect of the neutron transfer is an indirect effect of the quadrupole deformation. When after the neutron transfer the deformations of nuclei do not change or slightly decrease, the neutron transfer weakly influences or suppresses the capture cross section. Good examples for this effect are the capture reactions ${}^{60}\text{Ni} + {}^{100}\text{Mo}$, ${}^{150}\text{Nd}$, ${}^{18}\text{O} + {}^{64}\text{Ni}$, ${}^{112,114,116,118,120,122,124}\text{Sn}$, ${}^{204,206}\text{Pb}$, and ${}^{32}\text{S} + {}^{96}\text{Zr}$, ${}^{94,96,98,100}\text{Mo}$, ${}^{100,102,104}\text{Ru}$, ${}^{104,106,108,110}\text{Pd}$, ${}^{112,114,116,118,120,122,124}\text{Sn}$. at sub-barrier energies. Thus,

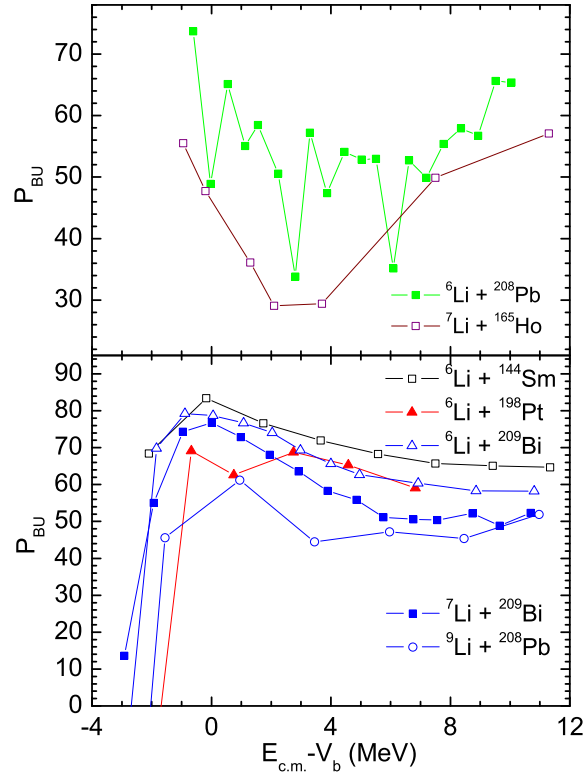


FIG. 16: (Color online) The same as in Fig. 15, but for the indicated reactions with ${}^{6,7,9}\text{Li}$ -projectiles.

the general point of view that the sub-barrier capture (fusion) cross section strongly increases because of the neutron transfer with a positive Q -values has to be revised.

The neutron transfer effect can lead to a weak influence of halo-nuclei on the capture. Comparing the capture cross sections calculated without the breakup effect and experimental complete fusion cross sections, the breakup was analyzed in reactions with weakly bound projectiles. A trend of a systematic behavior for the complete fusion suppression as a function of the target charge and bombarding energy is not achieved. The quasi-elastic or elastic backscattering was suggested to be an useful tool to study the behavior of the breakup probability.

We thank P.R.S. Gomes and A. Lepina-Szilny for fruitful discussions and suggestions. This work was supported by DFG, NSFC, RFBR, and JINR grants. The IN2P3(France)-JINR(Dubna) and Polish - JINR(Dubna) Cooperation Programmes are gratefully acknowledged.

-
- [1] L.F. Canto, P.R.S. Gomes, R. Donangelo, and M.S. Hussein, *Phys. Rep.* **424**, (2006) 1.
 - [2] V.V. Sargsyan, G.G. Adamian, N.V. Antonenko, and W. Scheid, *Eur. Phys. J. A* **45**, 125 (2010).
 - [3] V.V. Sargsyan *et al.*, *Eur. Phys. J. A* **47**, 38 (2011); **48**, 118 (2012); **49**, 19 (2013).
 - [4] V.V. Sargsyan *et al.*, *Phys. Rev. C* **84**, 064614 (2011).
 - [5] V.V. Sargsyan *et al.*, *Phys. Rev. C* **85**, 024616 (2012); *Eur. Phys. J. A* **49**, 54 (2013).
 - [6] V.V. Sargsyan *et al.*, *Phys. Rev. C* **86**, 014602 (2012).
 - [7] S. Szilner *et al.*, *Phys. Rev. C* **76**, 024604 (2007); S. Szilner *et al.*, *Phys. Rev. C* **84**, 014325 (2011); L. Corradi *et al.*, *Phys. Rev. C* **84**, 034603 (2011).
 - [8] C.H. Dasso, S. Landowne, and A. Winther, *Nucl. Phys.* **A405**, 381 (1983).
 - [9] G.G. Adamian, A.K. Nasirov, N.V. Antonenko, and R.V. Jolos, *Phys. Part. Nucl.* **25**, 583 (1994); K. Washiyama, D. Lacroix, and S. Ayik, *Phys. Rev. C* **79**, 024609 (2009).
 - [10] S. Raman, C.W. Nestor, Jr, and P. Tikkanen, *At. Data Nucl. Data Tables* **78**, 1 (2001).
 - [11] H. Timmers *et al.*, *Nucl. Phys.* **A633**, 421 (1998).
 - [12] F. Scarlassara *et al.*, *Nucl. Phys.* **A672**, 99 (2000).
 - [13] Z. Kohley *et al.*, *Phys. Rev. Lett.* **107**, 202701 (2011).

- [14] J.F. Liang *et al.*, Phys. Rev. C **78**, 047601 (2008).
- [15] L.F. Canto *et al.*, Nucl. Phys. **A821**, 51 (2009); J. Phys. G **36**, 015109 (2009).
- [16] J.J. Kolata *et al.*, Phys. Rev. C **85**, 054603 (2012).
- [17] F. Scarlassara *et al.*, EPJ Web Conf. **17**, 05002 (2011).
- [18] R. Pengo *et al.*, Nucl. Phys. **A411**, 255 (1983).
- [19] A.M. Stefanini *et al.*, Phys. Rev. C **52**, R1727 (1995).
- [20] H.M. Jia *et al.*, Phys. Rev. C **86**, 044621 (2012).
- [21] E.F. Aguilera, J.J. Kolata, and R.J. Tighe, Phys. Rev. C **52**, 3103 (1995).
- [22] P. Jacobs, Z. Fraenkel, G. Mamane, and L. Tserruya, Phys. Lett. B **175**, 271 (1986).
- [23] V. Tripathi *et al.*, Phys. Rev. C **65**, 014614 (2001).
- [24] M. Alcorta *et al.*, Phys. Rev. Lett. **106**, 172701 (2011).
- [25] J.C. Mein *et al.*, Phys. Rev. C **55**, R995 (1997).
- [26] N. Keeley and N. Alamanos, Phys. Rev. C **75**, 054610 (2007).
- [27] A. Mukherjee *et al.*, Phys. Rev. C **75**, 044608 (2007).
- [28] R. Wolski *et al.*, Eur. Phys. J. A **47**, 111 (2011).
- [29] W. Loveland *et al.*, Phys. Rev. C **74**, 064609 (2006); A.M. Vinodkumar *et al.*, Phys. Rev. C **80**, 054609 (2009).
- [30] B. Balantekin and G. Kocak, *AIP Conf. Proc.* **1072**, 289 (2008).
- [31] V.V. Sargsyan *et al.*, Phys. Rev. C **86**, 054610 (2012).
- [32] A. Diaz-Torres, J. Phys. G **37**, 075109 (2010); Comp. Phys. Comm. **182**, 1100 (2011).
- [33] P.R.S. Gomes *et al.*, Phys. Rev. C **84**, 014615 (2011); P.R.S. Gomes, J. Lubian, and L.F. Canto, Phys. Rev. C **79**, 027606 (2009).
- [34] H. Timmers *et al.*, Nucl. Phys. **A584**, 190 (1995); H.Q. Zhang *et al.*, Phys. Rev. C **57**, R1047 (1998); A.A. Sonzogni *et al.*, Phys. Rev. C **57**, 722 (1998); O.A. Capurro *et al.*, Phys. Rev. C **61**, 037603 (2000); S. Santra *et al.*, Phys. Rev. C **64**, 024602 (2001); R.F. Simões *et al.*, Phys. Lett. B **527**, 187 (2002); S. Sinha *et al.*, Phys. Rev. C **64**, 024607 (2001); E. Piasecki *et al.*, Phys. Rev. C **65**, 054611 (2002).